Supplementary Table 1: Body composition of 12-week-old female *Cyp24a1*$^{+/+}$, *Cyp24a1*$^{+/-}$ and *Cyp24a1*$^{-/-}$ mice.

Genotype	*Cyp24a1*$^{+/+}$	*Cyp24a1*$^{+/-}$	*Cyp24a1*$^{-/-}$
Length (cm)	8.90 ± 0.34	8.92 ± 0.26	8.80 ± 0.24
Total weight (g)	20.73 ± 0.84	20.58 ± 0.83	20.93 ± 0.61
ASC fat (g)	0.25 ± 0.03	0.20 ± 0.04	0.18 ± 0.03
Visceral fat (g)	0.40 ± 0.04	0.43 ± 0.05	0.48 ± 0.09
PSC fat (g)	0.13 ± 0.03	0.18 ± 0.03	0.13 ± 0.03
Lean weight (g)	18.45 ± 0.80	18.58 ± 0.65	18.83 ± 0.58
Body fat (%)	3.76 ± 0.34	3.87 ± 0.43	3.72 ± 0.31
Lean mass (%)	89.00 ± 0.39	90.35 ± 1.07	89.95 ± 0.18
BMI (kg/m^2)	2.63 ± 0.09	2.59 ± 0.08	2.71 ± 0.11

Mice were weighed and anesthetized prior to cardiac puncture and dissection of body fat. Tail was omitted from body length. ASC, anterior subcutaneous; PSC, posterior subcutaneous; BMI, body mass index. Results are mean ± SEM; 4 mice per group.

Supplementary Table 2 : Gene expression monitoring by cDNA microarrays in fracture callus from *Cyp24a1*$^{+/-}$ or *Cyp24a1*$^{-/-}$ mice.

Gene Title	Gene ID	Function	F.C. (Null/Hz)
Small proline rich protein family	Sprr2a	involved in epithelial different.,increased in allergic reaction in bronchi	5,3
BC057627		metal binding, nucleic acid binding	5,2
Chemokine ligand 1	Cxcl1	Angiogenic chemokine (mouse homologue of IL-8)	2,59
1500002O20Rik		**no described function**	**2,39**
Tenascin N/maybe W	Tnn	W inhibits preOBs prolifer. & different. during endoch.oss.,increased in fracture repair	2,37
2310046K23Rik		**hypothetical protein of no described function**	**2,35**
1500016O10Rik		**no described function, Integral to membrane protein**	**2,23**
1110020A10Rik		**no described function**	**2**
5730419F03Rik		no described function, expressed in mouse skin	0,49
Histone deacytelase 4	HDAC4	regulates chondrocyte hypertrophy &endoch. bone formation by inh.of RunX2	0,48
2310009E04Rik		Carbohydrate kinase	0,452
2310009E04Rik		no described function	0,45
Mm.196290		Oligonucleotide/Oligosachharide-binding fold containing protein	0,44
U46068		no known function	0,42
Ectodysplasin A2 isoform receptor	Eda2r	involved in hair, sweat gland and teeth loss in humans and mice	0,412
SH3 domain protein D19	SH3d19	no described function, expressed in mouse skin	0,38
mouse ATPase p5 member	ATP13a3	ATPase activity in all tissues	0,38
Rufy1 RUN and FYVE domain 1	Rrad	lipid,metal,protein binding-involved in endocytosis $ protein transport & cell migration	0,27
Keratin 8	Krt8	Intermediate filament protein involved in epithelial cytoskeletal organization	0,18
similar to keratin, cytokeratin 8	LOC434261	no described function	0,16
similar to keratin, cytokeratin 8	LOC675884	no described function	0,157
Keratin 18	Krt18	Intermediate filament protein involved in epithelial cytoskeletal organization	0,15
TGF-beta 1 induced transcript 4	TSC22	involved in ocular, maxilla,mandible,skull, and facial gland development	0,1

Total RNA was extracted from callus tissue of *Cyp24a1*$^{+/-}$ (n = 3) and *Cyp24a1*$^{-/-}$ (n = 3) mice and used as input material for cDNA microarray expression monitoring on a GeneChip MOE430 2.0 (Affymetrix, Applied Biosystems). Three criteria were established to target candidate genes involved in mediating the 24,25$(OH)_2D_3$ effect: 1) overexpressed by at least 2-fold in null tissue versus heterozygous tissue; 2) encoding for a membrane-associated protein and 3) protein of unknown function at the time of the assay. Four candidates matched these criteria (in red bold letters) and were cloned and transfected in COS7 cells to verify their binding capacity to tritiated 24R,25$(OH)_2D_3$. Complete dataset submitted to Gene Expression Omnibus repository: accession number GSE112449.

SUPPLEMENTAL FIGURES AND LEGENDS

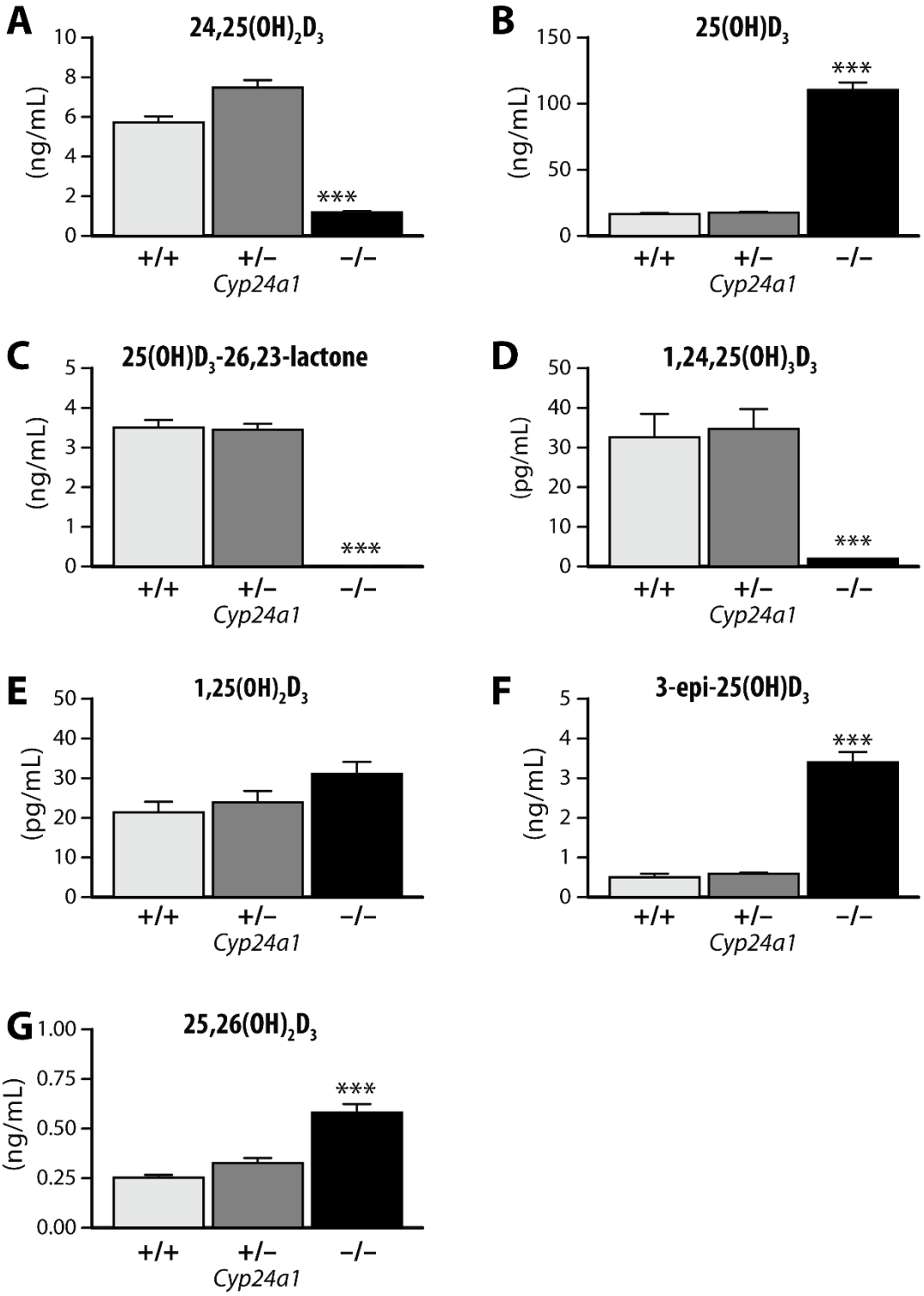

Supplemental Figure 1. Circulating levels of vitamin D metabolites in *Cyp24a1*$^{+/+}$, *Cyp24a1*$^{+/-}$ and *Cyp24a1*$^{-/-}$ female mice. Serum was isolated from whole blood harvested from 12-week-old mice and vitamin D metabolite levels (identified above each panel) were determined by LC-MS/MS following DMEQ-TAD derivatization. Three metabolites were below the detection limit of the assay in *Cyp24a1*$^{-/-}$ mice: 24,25-dihydroxyvitamin D_3 (**A**), 25-hydroxyvitamin D_3-26,23-lactone (**C**) and 1,24,25-trihydroxyvitamin D_3 (**D**). ***, $p < 0.001$, 1-way ANOVA followed by Bonferroni post-test, 5 animals per group.

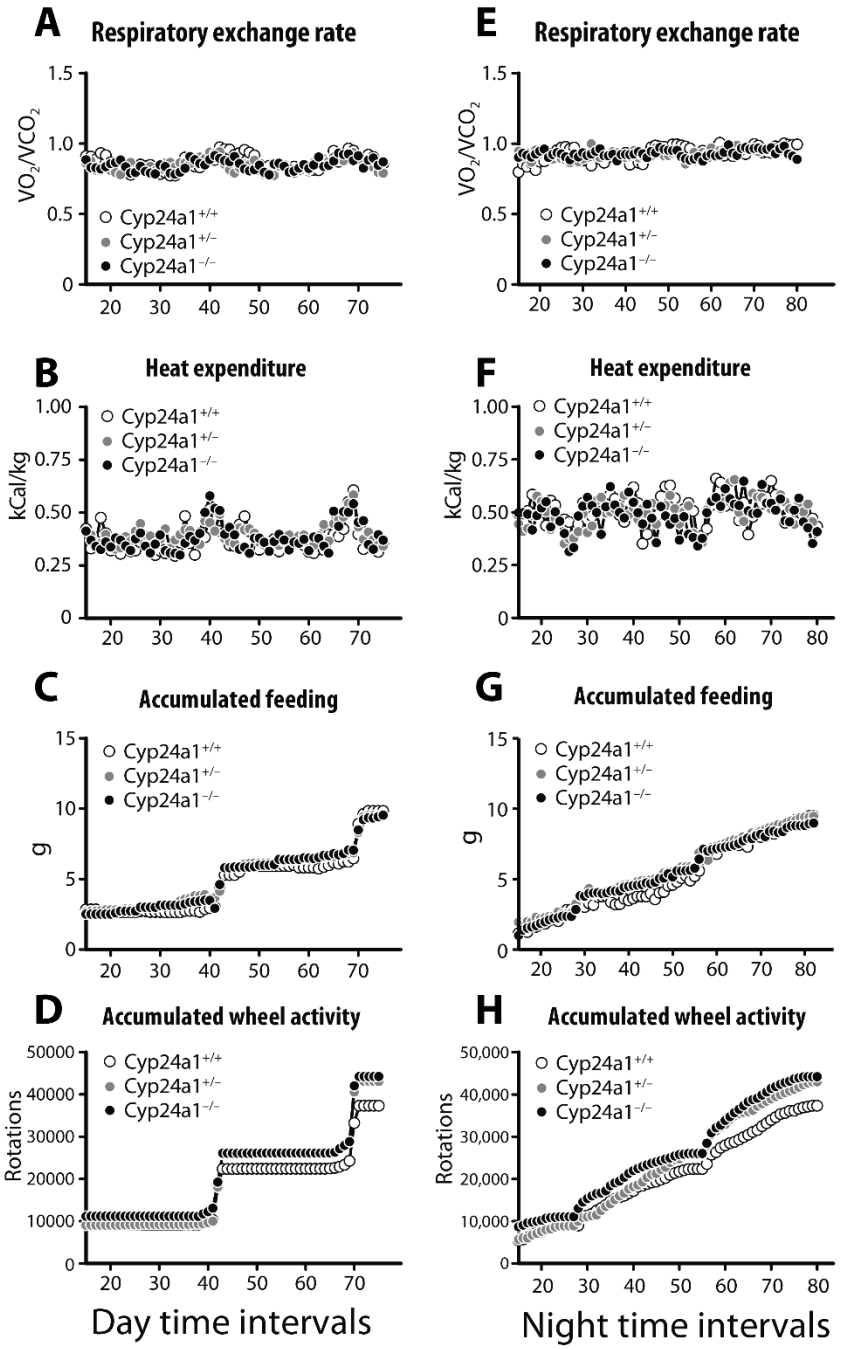

Supplemental Figure 2. Metabolic measurements in *Cyp24a1*$^{+/+}$, *Cyp24a1*$^{+/-}$ and *Cyp24a1*$^{-/-}$ mice. Twelve-week-old female mice were put in individual Oxymax metabolic chambers for 96 h. The system measured **(A, E)** respiratory exchange rate, **(B, F)** heat expenditure, **(C, G)** accumulated feeding and **(D, H)** accumulated wheel activity during day time **(A-D)** and night time **(E-H)** intervals. No significant difference was detected, repeated measures 2-way ANOVA followed by Bonferroni post-test, 4 animals per group.

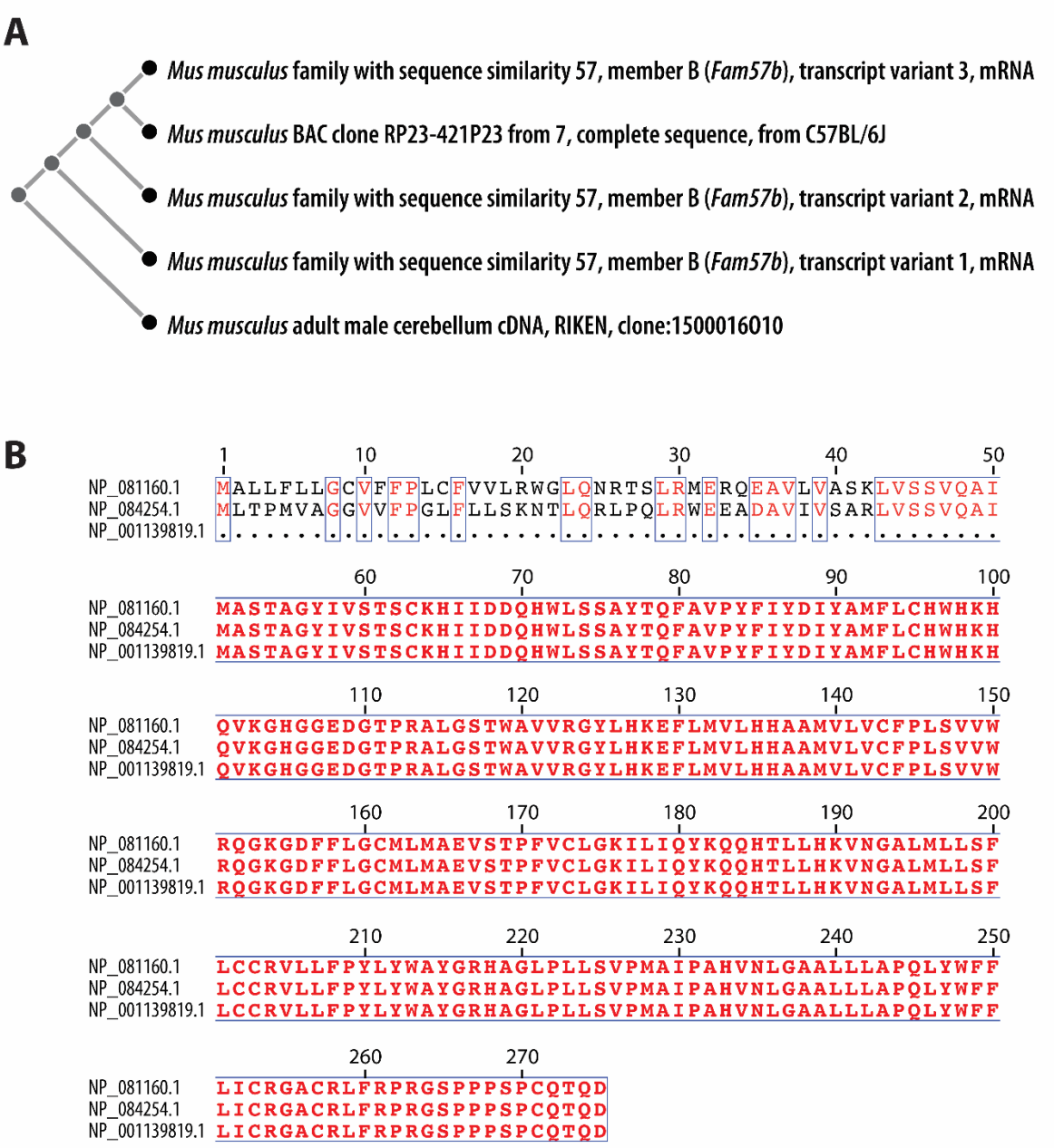

Supplemental Figure 3. BLAST analysis of Riken clone 1500016O10 from *Mus musculus* database and peptide sequences of FAM57B isoforms. (**A**) Distance tree of the matching sequences for Riken clone 1500016O10 following Blast analysis against the *Mus musculus* database. The distance tree was generated through the NIH Blast Tree View on-line widget https://www.ncbi.nlm.nih.gov/blast/treeview/.
(**B**) Peptide sequence alignment for the 3 FAM57B isoforms in *Mus musculus* with FAM57B2 (NP_081160.1) on top, FAM57B1 (NP_084254.1) in the middle, and FAM57B3 (NP_001139819.1) at the bottom. The 3 splice variants differ in their first 50 amino acid residues. The alignment was performed with the EsPript 3.0 on-line freeware http://espript.ibcp.fr/ESPript/cgi-bin/ESPript.cgi.

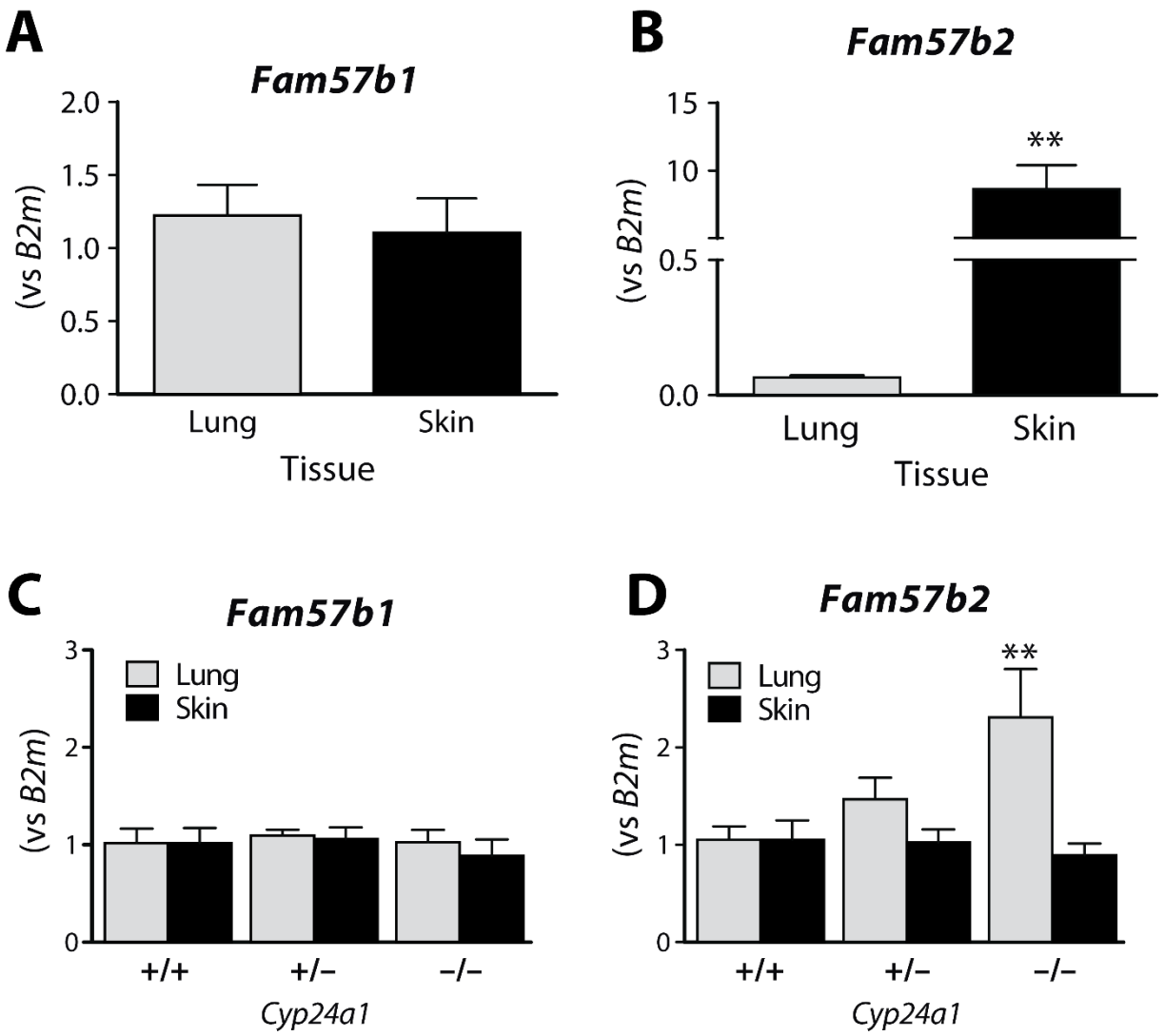

Supplemental Figure 4. Relative expression of *Fam57b1* and *Fam57b2* isoforms in lung and skin tissues of *Cyp24a1*$^{+/+}$, *Cyp24a1*$^{+/-}$ and *Cyp24a1*$^{-/-}$ mice. Total RNA was extracted from 12-week-old female mice and used to compared *Fam57b* isoform expression in lung and skin tissue. (**A, B**) Expression levels in wild-type (*Cyp24a1*$^{+/+}$) tissues relative to β2-microglobulin (B2m). **, p<0.01, 2-tailed t-test. (**C, D**) Expression levels across genotypes, normalized to B2m and expressed relative to +/+ levels arbitrarily assigned a value of 1. **, p < 0.01, 2-way ANOVA followed by Bonferroni post-test. Five animals per group.

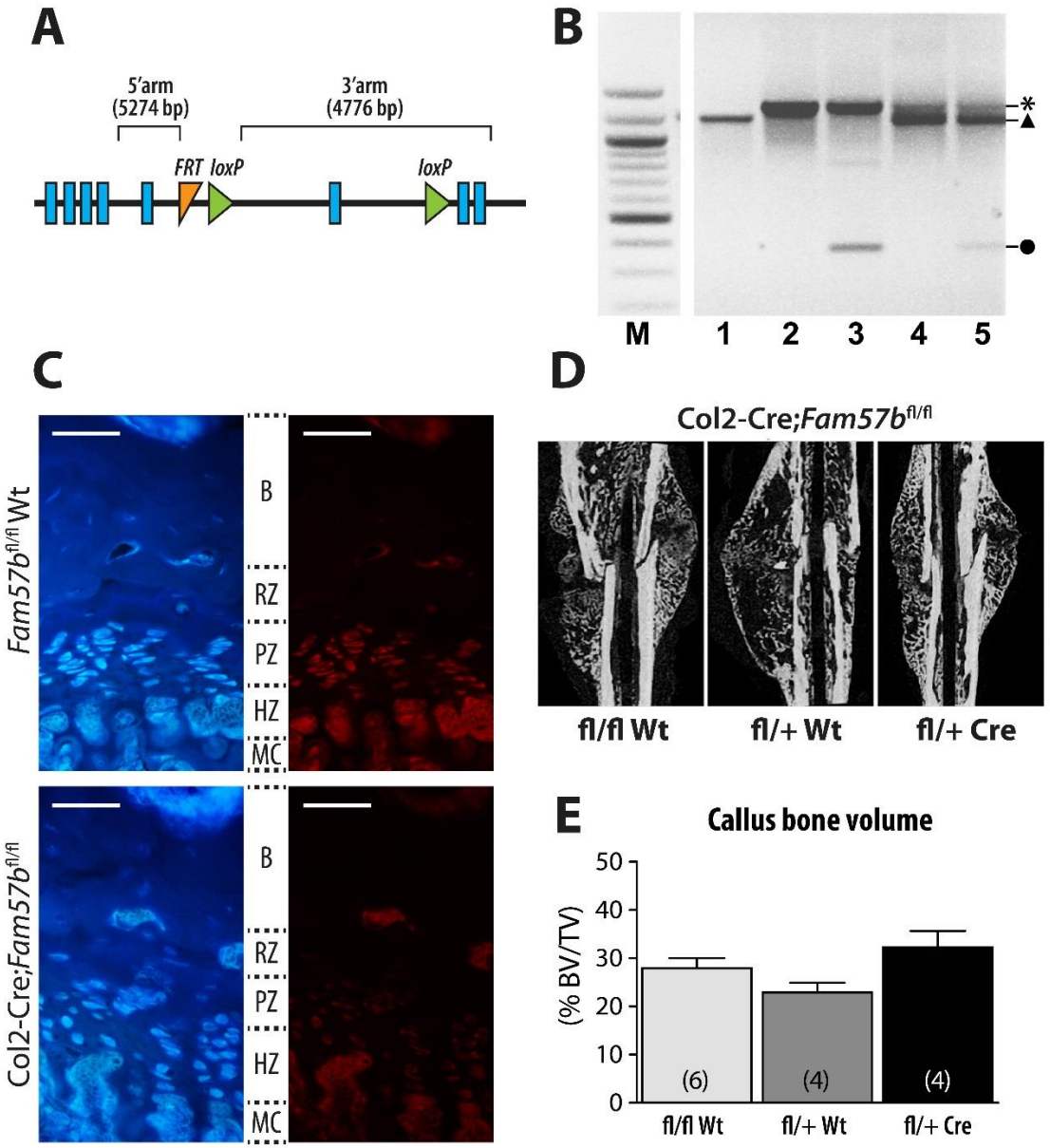

Supplemental Figure 5. Generation of Col2-Cre;*Fam57b*$^{fl/fl}$ mice. (A) Targeted allele showing floxed exon 6 (not to scale). The selection cassette was excised by crossing the floxed mice with a CMV-Flpe transgenic mouse, leaving a single FRT site. **(B)** Genotyping of tail snips from progeny. Amplimers from wild-type (▲), floxed (*), and excised (●) alleles are shown. M, molecular size markers. A representative litter is shown: lane 1, wild-type (+/+) littermate; lane 2, floxed/floxed (fl/fl); lane 3, Col2- Cre;floxed/floxed (fl/fl Cre); lane 4, floxed/+ (fl/+); lane 5, Col2-Cre;floxed/+ (fl/+ Cre). **(C)** FAM57B immunofluorescence on tibial growth plate sections of undecalcified methyl methacrylate-embedded bone sections from 8-week-old *Fam57b*$^{fl/fl}$ wt and Col2-Cre;*Fam57b*$^{fl/fl}$ female mice. Detection was with a 1:300 dilution of rabbit polyclonal anti-FAM57B antibody (catalog nb. Orb183613, Biorbyt, San Franscisco, CA) followed by 1:1000 Alexa594-conjugated goat anti-rabbit secondary antibody (catalog nb. A11012, Invitrogen) in 5% goat serum PBS. Images were obtained using a Leica DMR fluorescence microscope (Leica Microsystems, Wetzlar, Germany) connected to a digital DP70 camera (Olympus, Center Valley, PA). Image processing included whole image channel filtering to remove noise and whole image adjustment of brightness, contrast, color balance, and sharpening using Adobe Photoshop v. 12.1. Photoshop images were then flattened and imported into Adobe Illustrator v. 15.1 to build the final montages. B, Bone; RZ, resting zone; PZ, proliferating zone; HZ, hypertrophic zone; MC, mineralized cartilage. Magnification bar, 50 μm. **(D)** The calluses of all control genotypes (*Fam57b*$^{+/fl}$, fl/+ Wt; *Fam57b*$^{fl/fl}$, fl/fl Wt; and Col2-Cre;*Fam57b*$^{+/fl}$, fl/+ Cre) were analyzed to ensure that the floxed allele itself and Cre expression and excision produced no phenotype. Typical microCT raw images shown here for females on D14 post-osteotomy. **(E)** Analysis of relative bone volume from *Fam57b*$^{fl/fl}$ (fl/fl Wt), *Fam57b*$^{+/fl}$ (fl/+ Wt), and Col2-Cre;*Fam57b*$^{+/fl}$ (fl/+ Cre) calluses on D14 post-osteotomy. All p values>0.05, 1-way ANOVA followed by Bonferroni post-test. Number of animals per groups is indicated in parentheses.

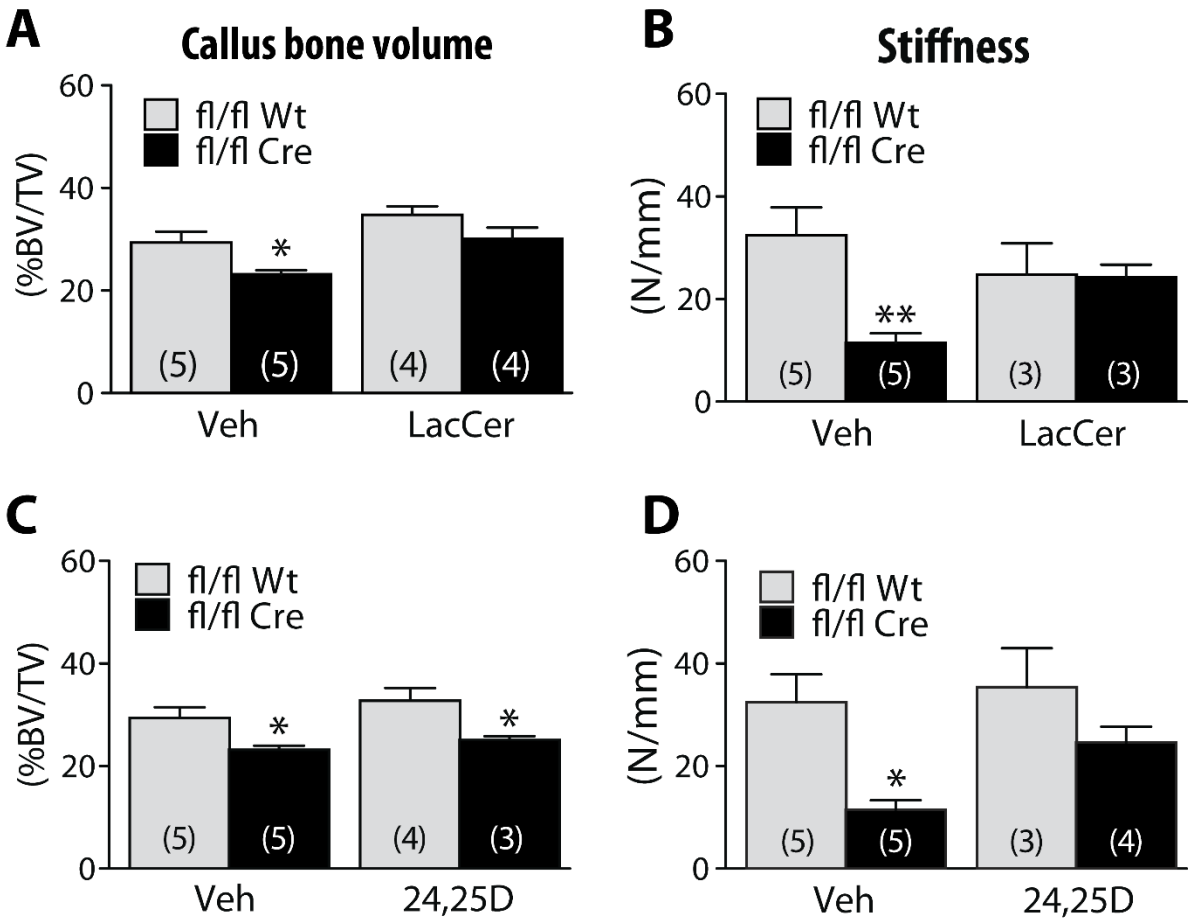

Supplemental Figure 6. Rescue treatment with 24R,25(OH)$_2$D$_3$ or lactosylceramide in male Col2-Cre;*Fam57b*$^{fl/fl}$ mice. Control (fl/fl Wt) and mutant (fl/fl Cre) male mice were subcutaneously injected for 15 days starting 72 h post-surgery with vehicle (Veh), 6.7 µg/kg daily of 24R,25(OH)$_2$D$_3$ (24,25D), or 50 µg/kg daily of C18-lactosylceramide (LacCer). Bone volume (**A**, **C**) was calculated by microcomputed tomography. Stiffness (**B**, **D**) was calculated from the 3-point bending test. *, $p<0.05$; **, $p<0.01$, 2-way ANOVA followed by Bonferroni post-test. Number of animals per group is indicated in parentheses.

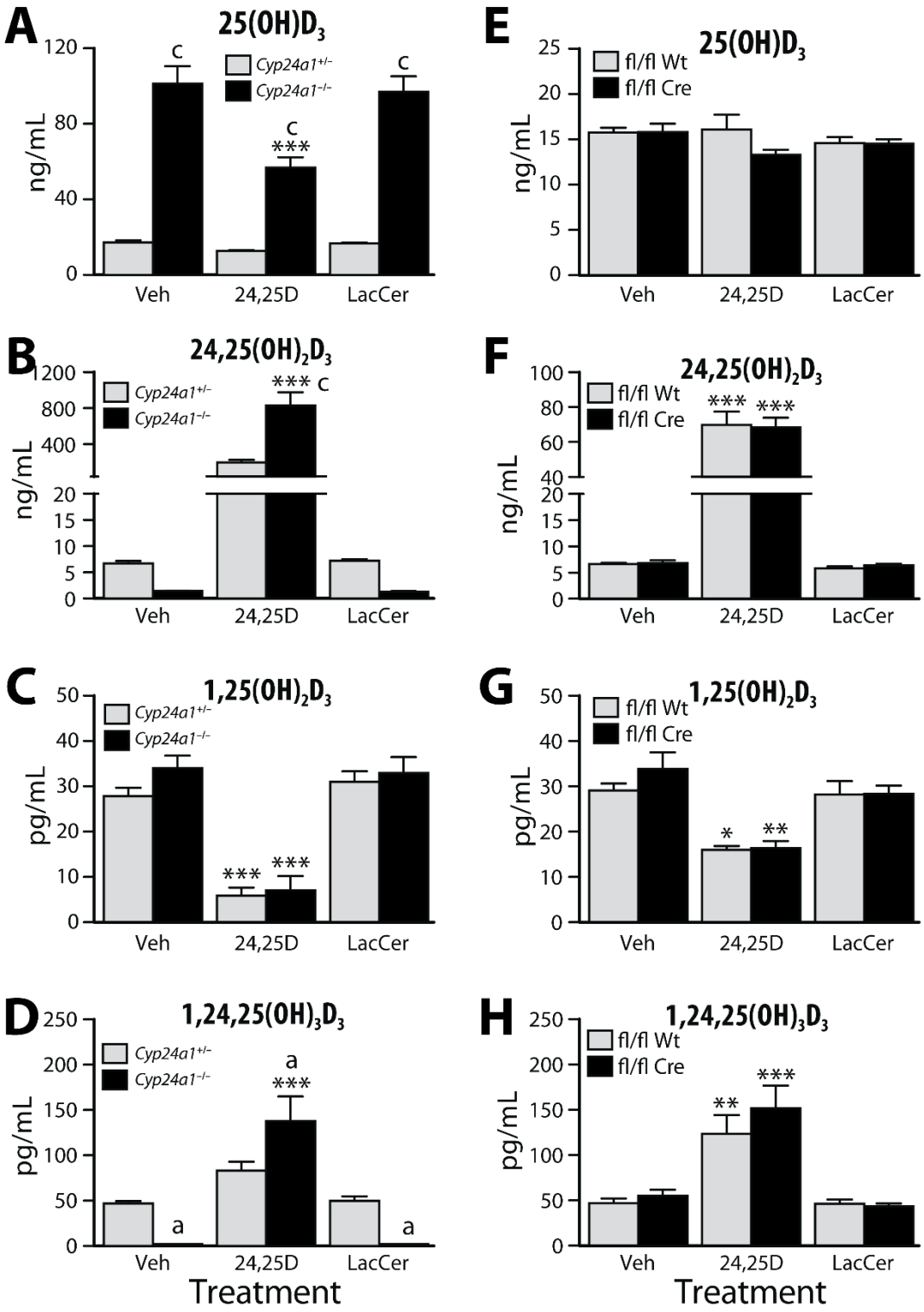

Supplemental Figure 7. Effect of 24R,25(OH)$_2$D$_3$ or lactosylceramide in vivo rescue on levels of main vitamin D metabolites. Serum levels of **(A, E)** 25(OH)D$_3$, **(B, F)** 24R,25(OH)$_2$D$_3$, **(C, G)** 1,25(OH)$_2$D$_3$ and **(D, H)** 1,24,25(OH)$_3$D$_3$ were determined by DMEQ-TAD derivatization coupled to LC-MS/MS in control and mutant *Cyp24a1* **(A-D)** and *Fam57b*$^{fl/fl}$ **(E-H)** mice. fl/fl Wt, controls; fl/fl Cre, mutants. *, p<0.05; **, p<0.01; ***, p<0.001 versus genotype-matched vehicle (veh); a, p<0.05; c, p<0.001 mutant versus control genotype, 2-way ANOVA followed by Bonferroni, 6 animals per group.